Toward accurate CO_2 and CH_4 observations from GOSAT

A. Butz,[1,2] S. Guerlet,[2] O. Hasekamp,[2] D. Schepers,[2] A. Galli,[2] I. Aben,[2] C. Frankenberg,[3] J.-M. Hartmann,[4] H. Tran,[4] A. Kuze,[5] G. Keppel-Aleks,[6] G. Toon,[3] D. Wunch,[6] P. Wennberg,[6] N. Deutscher,[7,8] D. Griffith,[7] R. Macatangay,[7] J. Messerschmidt,[8] J. Notholt,[8] and T. Warneke[8]

Received 21 April 2011; revised 14 June 2011; accepted 20 June 2011; published 30 July 2011.

[1] The column-average dry air mole fractions of atmospheric carbon dioxide and methane (X_{CO_2} and X_{CH_4}) are inferred from observations of backscattered sunlight conducted by the Greenhouse gases Observing SATellite (GOSAT). Comparing the first year of GOSAT retrievals over land with colocated ground-based observations of the Total Carbon Column Observing Network (TCCON), we find an average difference (bias) of −0.05% and −0.30% for X_{CO_2} and X_{CH_4} with a station-to-station variability (standard deviation of the bias) of 0.37% and 0.26% among the 6 considered TCCON sites. The root-mean square deviation of the bias-corrected satellite retrievals from colocated TCCON observations amounts to 2.8 ppm for X_{CO_2} and 0.015 ppm for X_{CH_4}. Without any data averaging, the GOSAT records reproduce general source/sink patterns such as the seasonal cycle of X_{CO_2} suggesting the use of the satellite retrievals for constraining surface fluxes. **Citation:** Butz, A., et al. (2011), Toward accurate CO_2 and CH_4 observations from GOSAT, *Geophys. Res. Lett.*, *38*, L14812, doi:10.1029/2011GL047888.

1. Introduction

[2] Space-based remote sensing of the CO_2 and CH_4 column-average dry air mole fractions (X_{CO_2} and X_{CH_4}) has the potential to provide global observational constraints on CO_2 and CH_4 fluxes across the surface-atmosphere boundary and to foster insight into the related biogeochemical cycles. However, measurements of X_{CO_2} and X_{CH_4} face challenging accuracy requirements. The target accuracy for regionally and weekly averaged X_{CO_2} and X_{CH_4} is on the order of a few tenths of a percent out of background concentrations of roughly 385 ppm (parts per million) and 1.8 ppm, respectively, where the requirement for X_{CH_4} is somewhat less stringent than for X_{CO_2} [e.g., *Chevallier et al.*, 2007; *Meirink et al.*, 2006].

[3] Currently, the SCanning Imaging Absorption spectroMeter for Atmospheric CartograpHY (SCIAMACHY), in orbit since 2002, and the Greenhouse gases Observing SATellite (GOSAT), in orbit since January 2009, aim at achieving this goal by exploiting absorption spectra of backscattered sunlight in the shortwave-infrared (SWIR) spectral range. SCIAMACHY has been shown to provide accurate X_{CO_2} [e.g., *Reuter et al.*, 2011] and X_{CH_4} [e.g., *Frankenberg et al.*, 2005] if lightpath modification due to scattering by atmospheric particles is taken into account by the retrieval methods. First retrievals from GOSAT have been reported by *Yoshida et al.* [2011] and *Morino et al.* [2011]. They use relatively weak CO_2 and CH_4 absorption bands (~6100 cm^{-1}) in combination with the O_2A-band (~13,000 cm^{-1}) to retrieve X_{CO_2}, X_{CH_4}, and simultaneously the amount of a predefined aerosol type in the boundary layer. Validation of their results by ground-based measurements of the Total Carbon Column Observing Network (TCCON) [*Wunch et al.*, 2011] shows a standard deviation of the differences of generally more than 1%, which is too large to unambiguously identify characteristic source/sink patterns such as the seasonal cycle of X_{CO_2}. This shortcoming might be partly due to lightpath modification not only depending on the particle amount but also on particle size and height.

[4] Here we demonstrate that we can deliver retrievals of X_{CO_2} and X_{CH_4} from GOSAT with improved quality and that timeseries of individual GOSAT retrievals allow for identifying characteristic source/sink patterns. This is achieved using the O_2A-band, the weak CO_2 and CH_4 absorption bands around 6100 cm^{-1}, and the strong CO_2 and H_2O absorption bands around 4850 cm^{-1} in order to simultaneously retrieve information on the particle amount, size, and height, together with X_{CO_2} and X_{CH_4}. The quality of the retrieval results is evaluated through comparison with coinciding ground-based observations at 6 TCCON sites.

2. GOSAT Observations and Auxiliary Data

[5] The Thermal And Near infrared Sensor for carbon Observation (TANSO) - Fourier Transform Spectrometer (FTS) onboard GOSAT observes sunlight backscattered by the Earth's surface and atmosphere in 3 channels covering the SWIR spectral range. A further channel records thermal radiation in the longwave infrared, which is not used here. Over land, the instrument collects light about the nadir (±35° across track, ±20° along track). Over the ocean, it also looks at the glint spot, the point of specular reflection at the water

[1] Institute for Meteorology and Climate Research, Karlsruhe Institute of Technology, Leopoldshafen, Germany.
[2] Netherlands Institute for Space Research, Utrecht, Netherlands.
[3] Jet Propulsion Laboratory, California Institute of Technology, Pasadena, California, USA.
[4] Laboratoire Interuniversitaire des Systèmes Atmosphériques, UMR 7583, CNRS, Université Paris-Est Créteil, Université Paris Diderot, Institut Pierre-Simon Laplace, Créteil, France.
[5] Japan Aerospace Exploration Agency, Tsukuba, Japan.
[6] Division of Engineering and Applied Science, California Institute of Technology, Pasadena, California, USA.
[7] Center for Atmospheric Chemistry, University of Wollongong, Wollongong, New South Wales, Australia.
[8] Institute of Environmental Physics, University of Bremen, Bremen, Germany.

0094-8276/11/2011GL047888

surface. The FTS has a maximum optical path difference of 2.5 cm and an instantaneous field-of-view of 15.8 mrad mapping into a spectral resolution of ~0.3 cm^{-1} and a circular footprint with ~5 km radius at the sub-satellite point. Backscattered sunlight is recorded in 2 orthogonal polarization directions from which we calculate the total backscattered radiance (Stokes parameter I) as suggested by *Yoshida et al.* [2011]. The radiometric calibration of the spectra is based on the Mueller matrix calculus of *Kuze et al.* [2009] and the pre-launch measured calibration data (with corrections) available from GOSAT's instrument support. The latter also provides the tabulated instrument line shape (ILS) used by our algorithm. The TANSO-Cloud and Aerosol Imager (CAI), the other instrument onboard GOSAT, delivers cloud flags for several hundred ground pixels within a single TANSO-FTS footprint which we use for cloud screening (see auxiliary material for details).[1]

[6] Further auxiliary information necessary to accurately retrieve X_{CO_2} and X_{CH_4} is collected by a preprocessing step. Vertical profiles of pressure, temperature, and humidity as well as surface pressure and wind speeds are extracted from the ECMWF (European Centre for Medium-Range Weather Forecasts) ERA-Interim analysis provided 6-hourly on a 1.5° × 1.5° latitude × longitude grid. ERA-Interim fields are interpolated to the time and center location of the TANSO-FTS footprint taking into account surface elevation and its variability through the GTOPO30 database. The initial guess for the CO_2 and CH_4 vertical concentration profiles is taken from CarbonTracker [*Peters et al.*, 2007] and TM4 [*Meirink et al.*, 2006] model runs for the year 2008 and 2007, respectively.

3. Retrieval Method

[7] The retrieval method has been described in detail by *Butz et al.* [2009, 2010]. The key quality of the method is its ability to simultaneously retrieve gas concentrations and particle scattering properties of the atmosphere using an efficient radiative transfer (RT) model [*Hasekamp and Butz*, 2008]. Particle scattering properties are effectively parameterized by a single spherical particle type characterized through its total column number density N_s, the size distribution parameter α_s, the height distribution parameter z_s, and a fixed-value refractive index (1.400-i × 0.003). Thereby, the particle number density size distribution follows a power-law $\propto r^{-\alpha_s}$ with r the particle radius. The height distribution of particle optical thickness is a Gaussian function of center height z_s.

[8] Molecular absorption lines of O_2 and CO_2 are modeled by a spectroscopic model that includes line-mixing as well as collision-induced-absorption by O_2 [*Tran and Hartmann*, 2008; *Lamouroux et al.*, 2010]. Absorption of CH_4 and the interfering absorber H_2O is modeled by feeding HITRAN 2008 [*Rothman et al.*, 2009] spectroscopic parameters into a Voigt lineshape model. Solar Fraunhofer lines are represented through an empirical linelist (G. Toon, JPL, personal communication, 2011). For nadir-view, surface reflection is assumed Lambertian, while for ocean-glint view, a wind-speed driven Cox-and-Munk surface model [*Cox and Munk*, 1954] is combined with a Lambertian albedo slope.

[9] Here, we run the RT model in scalar mode, i.e., we neglect polarization of radiation and only calculate the total radiance (Stokes parameter I) backscattered to the satellite observer. Given the RT modeled and the measured radiances, an inverse method based on Phillips-Tikhonov regularization in combination with the L-curve method estimates the retrieval parameters. We exploit radiances in the 4 windows covering the O_2A-band ([12920,13195] cm^{-1}), a weakly absorbing CO_2 band ([6170,6278] cm^{-1}), a CH_4 band ([6045,6138] cm^{-1}), and a strongly absorbing CO_2 band ([4806,4896] cm^{-1}). Retrieval parameters are the 12-layer vertical profiles of the CO_2 and CH_4 column number densities, the total column number density of the interfering absorber H_2O, the scattering parameters N_s, α_s, and z_s, a 2nd order polynomial for surface albedo per window, and spectral shift parameters per window. Further, we retrieve a constant offset that adds to the radiance in the O_2A-band window in order to effectively account for uncorrected non-linearity of the analogue-to-digital converter and contributions from plant fluorescence [*Frankenberg et al.*, 2011].

[10] The target quantities X_{CO_2} and X_{CH_4} are calculated by summing the respective column number densities over the 12 retrieval layers and dividing by the dry air column. The latter is calculated from the ECMWF meteorological support. Except for calibration purposes (section 4), we do not retrieve the dry air column or a related quantity such as surface pressure.

4. Calibrating O_2

[11] Our retrieval method relies on accurate modeling of the O_2A-band which provides a large part of the information content on atmospheric scattering properties. Therefore, we first investigate whether our model of the O_2A-band is consistent with the measurements before aiming at X_{CO_2} and X_{CH_4} retrievals.

[12] To this end, we require TANSO-FTS O_2A-band spectra that are not affected by aerosol and cloud scattering, and thus only depend on O_2 absorption and surface reflection. Ocean-glint observations allow for selecting such spectra. We set up a simplified version of our method, that retrieves the O_2 total column number density ($[O_2]$) and the near surface windspeed from ocean-glint observations of the O_2A-band ([12920,13195] cm^{-1}) alone. The simplified forward model only accounts for Rayleigh scattering by molecules but neglects scattering by particles. For ocean glint observations, the latter assumption leads always to an underestimation of the retrieved $[O_2]$ due to unaccounted lightpath shortening if scattering particles are present in the atmosphere. Overestimation of retrieved $[O_2]$ does not occur since scattering induced lightpath enhancement typically requires a reflection at the ground which is inefficient due to low reflectivity of the ocean surface for off-glint angles [*Aben et al.*, 2007].

[13] Figure 1 illustrates the ratio of retrieved $[O_2]$ to the ECMWF $[O_2]$ estimate for TANSO-FTS ocean-glint measurements between June 1, 2009, and August 31, 2009. A cloud of low $[O_2]$ retrievals is bound by a sharp 'upper edge'. Low-biased $[O_2]$ relates to scattering effects as explained above. The 'upper edge' consists of scenes where the particle load is low and scattering effects are negligible. If the retrieval model of the O_2A-band was consistent with the measurements, $[O_2]$ retrievals along the 'upper edge' should be in agreement with the ECMWF estimate. However, we find a

[1] Auxiliary materials are available in the HTML. doi:10.1029/2011GL047888.

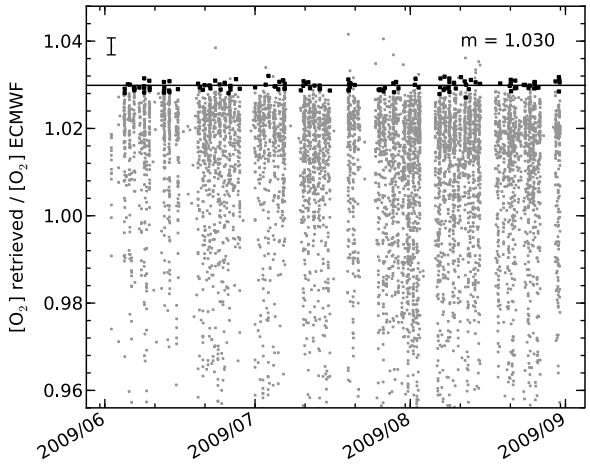

Figure 1. Ratio of $[O_2]$ retrieved from TANSO-FTS ocean-glint observations to $[O_2]$ calculated from ECMWF meteorological input. We show all individual retrievals (grey) between June 1, 2009, and August 31, 2009, after some basic quality filtering. Data contributing to the 'upper edge' (black dots) are used to fit a constant m (solid line). The 'upper edge' is defined such that ~32% of the data above the fitted constant deviate by more than the 1-sigma noise error from the fit. For clarity, only a typical errorbar representing the 1-sigma noise error of the satellite retrievals is given in the upper left corner.

scaling factor of 1.030 between retrieved $[O_2]$ and ECMWF $[O_2]$ as determined by a least-squares fit of a constant to the 'upper edge'.

[14] The origin of the detected scaling factor remains unclear so far but is most likely attributable to spectroscopic uncertainties. Irrespective of the actual origin of the inconsistency, we scale the O_2 absorption cross sections in the O_2A-band by a factor 1.030 to make our O_2A-band model consistent with the observations.

5. Validating CO_2 and CH_4

[15] For validation of our X_{CO_2} and X_{CH_4} retrievals from TANSO-FTS, we consider roughly the first year of satellite operation between April 2009 and July 2010. We focus on satellite observations in the vicinity of 6 TCCON sites in North-America (Lamont, 36.6°N 97.5°W; Park Falls, 45.9°N 90.3°W), Australia (Darwin, 12.4°S 130.9°E; Wollongong, 34.4°S 150.9°E), and Europe (Bialystok, 53.2°N 23.0°E; Orleans, 48.0°N 2.1°E). At each TCCON site, a ground-based sun-viewing FTS provides highly accurate estimates of X_{CO_2} and X_{CH_4} calibrated to the WMO standard [*Deutscher et al.*, 2010; *Messerschmidt et al.*, 2010; *Wunch et al.*, 2010]. Unavailability of validation data is typically due to local cloud cover omitting direct sun-viewing and due to periods of instrument maintenance.

[16] We process TANSO-FTS spectra which are recorded in nadir-view over land within 5° latitude/longitude radius of the considered TCCON stations. Observations are *a priori* filtered according to several criteria such as cloudiness of the scene, instrumental error flags, extreme viewing geometry, surface roughness, and signal-to-noise. *A posteriori*, we reject bad quality fits and difficult scattering scenes based on a 'scattering' criterion $\tau_s \times 1/\alpha_s \times z_s[\text{km}] > 0.3$ where the filter threshold 0.3 is determined empirically and τ_s is the retrieved particle optical thickness (at the O_2A-band) (see auxiliary material for details).

[17] Figure 2 compares the time series of X_{CO_2} and X_{CH_4} retrieved from TANSO-FTS to the validation data provided by TCCON. The diurnal range of TCCON data reflects the variability of airmass transport and source/sink processes as well as the effect of measurement errors [*Keppel-Aleks et al.*, 2011]. For calculating the bias and scatter of the satellite retrievals per station, a temporal coincidence criterion is applied (maximum 2 h mismatch between satellite and ground-based observations). Among the 6 validation sites, the overall bias of the X_{CO_2} satellite retrievals is −0.05% with a station-to-station variability of 0.37% (standard deviation of the bias). The X_{CH_4} retrievals exhibit an overall bias of −0.30% and a station-to-station variability of 0.26%. X_{CH_4} retrievals at Bialystok seem exceptionally high in comparison to the other stations. Excluding the Bialystok record from the statistics reduces the station-to-station variability of the X_{CH_4} satellite record to 0.12% with an average bias of −0.34%. As a measure of the scatter in our satellite retrievals, we calculate the root-mean-square deviation of the bias-corrected satellite record from the colocated TCCON data. The average scatter of X_{CO_2} and X_{CH_4} amounts to 2.8 ppm and 0.015 ppm among the 6 validation sites which is roughly twice the combined noise error estimated by the satellite and ground-based retrievals. The comparison for Wollongong reveals a large scatter of the TANSO-FTS retrievals for both target species which could be related to rough surface topography in Wollongong's vicinity. Slight errors in the geolocation of the TANSO-FTS footprint could cause errors in assumed surface elevation and surface pressure and thus map into X_{CO_2} and X_{CH_4} errors. In general, statistics and conclusions are most robust for the Lamont site since data availability is high throughout the year. For the other stations, the applied filtering causes significant gaps in the satellite record which hinder the statistical analysis.

[18] In comparison to a retrieval method that entirely neglects particle scattering, our refined method in particular yields a reduced scatter of the X_{CO_2} and X_{CH_4} retrievals and provides the 'scattering' criterion that efficiently screens outliers (see auxiliary material). The calibration of the O_2A-band absorption cross sections as proposed in section 4 substantially affects the retrieved scattering parameters. Among the validation ensemble, the retrieved scattering optical thickness (at the O_2A-band) is found reduced from on average 0.17 without O_2 scaling to 0.09 with O_2 scaling. The latter retrievals agree reasonably well with colocated ground-based measurements made by the Atmospheric Radiation Measurement (ARM) program at Lamont (see auxiliary material). The average scattering layer height is found increased from 3.3 km without O_2 scaling to 5.4 km with O_2 scaling. Generally, omitting the O_2 scaling results in a longer lightpath assumed by the retrieval method. Consequently, the retrieved X_{CO_2} and X_{CH_4} as shown in Figure 2 is lower by on average 0.21% and 0.27%, respectively, if O_2 scaling is omitted. Station-to-station variability and scatter are only slightly affected.

[19] In general, the satellite retrievals capture the temporal and spatial patterns observed in the validation data well. In particular, the Northern hemisphere seasonal cycle of X_{CO_2}

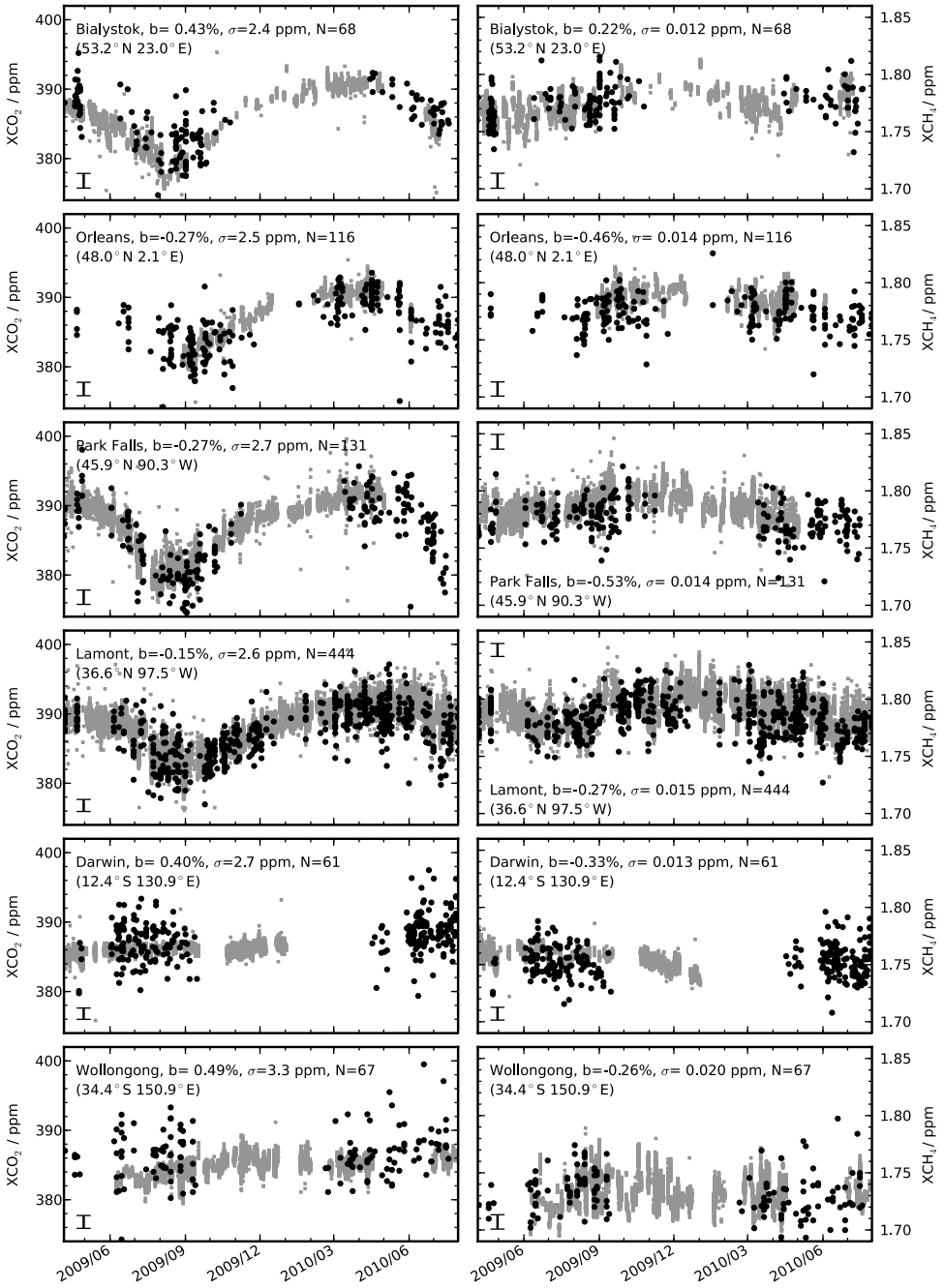

Figure 2. Time series of (left) X_{CO_2} and (right) X_{CH_4} retrievals from TANSO-FTS (solid black dots) in comparison to ground-based validation data (grey) provided by 6 TCCON stations (top to bottom ordered according to latitude). All validation data that pass the TCCON quality filters are shown. TANSO-FTS retrievals are *a priori* and *a posteriori* filtered as described in section 5. All valid TANSO-FTS retrievals within 5° latitude/longitude radius of the respective TCCON stations are depicted irrespective of the temporal mismatch between the ground-based and satellite measurements. For clarity, only a typical error bar representing the noise error of the satellite retrievals is given in the lower or upper left corner of each panel. Beside the name and the geolocation of the validation site, the panel legends quote the average bias b between TANSO-FTS retrievals and TCCON data, the root-mean-square deviation σ of the bias-corrected satellite record from the validation data, and the number N of data pairs considered for calculating these quantities. N is smaller than the plotted number of TANSO-FTS retrievals since a 2 h temporal coincidence criterion is applied in addition to the spatial criterion.

with the late summer minimum and the spring maximum is clearly discernible for Bialystok, Orleans, Park Falls, and Lamont. The seasonal cycle at Park Falls reveals the largest amplitude among the Northern hemisphere sites. As expected, the Southern hemisphere stations Darwin and Wollongong lack a pronounced X_{CO_2} seasonal cycle. The X_{CH_4} retrievals confirm the ~0.05 ppm difference between Northern and Southern hemisphere abundances. Seasonal patterns are less distinct for X_{CH_4} than for X_{CO_2} but variations such as a rapid increase of X_{CH_4} in late summer 2009 at Lamont are observable in TANSO-FTS and TCCON data.

6. Conclusion

[20] We process GOSAT observations between April 2009 and July 2010 by a method that allows for the simultaneous retrieval of X_{CO_2}, X_{CH_4}, and parameters representing the amount, the size, and the height of scattering particles in the atmosphere. Comparison of the inferred X_{CO_2} and X_{CH_4} to validation measurements at 6 ground-based TCCON sites around the world indicates that our satellite retrievals exhibit a residual bias and a station-to-station variability of the bias on the order of a few tenths of a percent for both, X_{CO_2} and X_{CH_4}. The scatter of our GOSAT retrievals is well below 1%. This is a substantial improvement compared to earlier GOSAT validation efforts [*Yoshida et al.*, 2011; *Morino et al.*, 2011]. The improved quality of our X_{CO_2} and X_{CH_4} retrievals allows for unambiguously identifying source/sink signals such as the seasonal cycle and its amplitude for X_{CO_2} and the interhemispheric gradient for X_{CH_4} without any data averaging. Constraining surface fluxes by our X_{CO_2} and X_{CH_4} GOSAT records is the logical next step.

[21] **Acknowledgments.** Access to GOSAT data was granted through the 2nd GOSAT research announcement jointly issued by JAXA, NIES, and MOE. Funding of this research came from the Dutch User Support Program under project GO-2005/064 and GO-AO/21 (DS), from ESA's CCI on GHGs and the European Commission's 7th framework program under grant agreement 218793 (SG), from DFG's Emmy-Noether program under project RemoteC BU2599/1-1 (AB). ECMWF ERA Interim analyses are provided through http://data-portal.ecmwf.int/data/d/interim_daily/. GTOPO30 is available from the U.S. Geological Survey through the Earth Resources Observation and Science (EROS) Center (http://eros.usgs.gov/#/Find_Data/Products_and_Data_Available/gtopo30_info). CarbonTracker data are provided by NOAA ESRL, Boulder, Colorado, USA from the Web site at http://carbontracker.noaa.gov. TM4 fields have been made available through Jan-Fokke Meirink, Royal Netherlands Meteorological Institute (KNMI). US funding for TCCON comes from NASA's Terrestrial Ecology Program (NNX08A186G), the Orbiting Carbon Observatory Program (NAS7-03001), the DOE/ARM Program and the Atmospheric CO_2 Observations from Space Program. Some of the research described in this paper was performed at the Jet Propulsion Laboratory, California Institute of Technology, under a contract with the NASA. We acknowledge the support of the European Commission within the 6th Framework Program through the Integrated Infrastructure Initiative IMECC and the Integrated Project GEOmon. We thank AeroMeteo Service, (Bialystok, Poland) and the RAMCES team at LSCE (Gif-sur-Yvette, France) for maintaining the Bialystok and Orleans FTS sites and providing station logistics.

[22] The Editor thanks two anonymous reviewers for their assistance in evaluating this paper.

References

Aben, I., O. Hasekamp, and W. Hartmann (2007), Uncertainties in the space-based measurements of CO_2 columns due to scattering in the Earth's atmosphere, *J. Quant. Spectrosc. Radiat. Transfer*, *104*, 450–459, doi:10.1016/j.jqsrt.2006.09.013.

Butz, A., O. P. Hasekamp, C. Frankenberg, and I. Aben (2009), Retrievals of atmospheric CO_2 from simulated space-borne measurements of back-scattered near-infrared sunlight: Accounting for aerosol effects, *Appl. Opt.*, *48*, 3322, doi:10.1364/AO.48.003322.

Butz, A., O. P. Hasekamp, C. Frankenberg, J. Vidot, and I. Aben (2010), CH_4 retrievals from space-based solar backscatter measurements: Performance evaluation against simulated aerosol and cirrus loaded scenes, *J. Geophys. Res.*, *115*, D24302, doi:10.1029/2010JD014514.

Chevallier, F., F.-M. Bréon, and P. J. Rayner (2007), Contribution of the Orbiting Carbon Observatory to the estimation of CO_2 sources and sinks: Theoretical study in a variational data assimilation framework, *J. Geophys. Res.*, *112*, D09307, doi:10.1029/2006JD007375.

Cox, C., and W. Munk (1954), Statistics of the sea surface derived from sun glitter, *J. Mar. Res.*, *13*, 198–227.

Deutscher, N. M., et al. (2010), Total column CO_2 measurements at Darwin, Australia—Site description and calibration against in situ aircraft profiles, *Atmos. Meas. Tech.*, *3*(4), 947–958, doi:10.5194/amt-3-947-2010.

Frankenberg, C., J. F. Meirink, M. van Weele, U. Platt, and T. Wagner (2005), Assessing methane emissions from global space-borne observations, *Science*, *308*, 1010–1014, doi:10.1126/science.1106644.

Frankenberg, C., A. Butz, and G. C. Toon (2011), Disentangling chlorophyll fluorescence from atmospheric scattering effects in O_2A-band spectra of reflected sun-light, *Geophys. Res. Lett.*, *38*, L03801, doi:10.1029/2010GL045896.

Hasekamp, O. P., and A. Butz (2008), Efficient calculation of intensity and polarization spectra in vertically inhomogeneous scattering and absorbing atmospheres, *J. Geophys. Res.*, *113*, D20309, doi:10.1029/2008JD010379.

Keppel-Aleks, G., P. O. Wennberg, and T. Schneider (2011), Sources of variations in total column carbon dioxide, *Atmos. Chem. Phys*, *11*(8), 3581–3593, doi:10.5194/acp-11-3581-2011.

Kuze, A., H. Suto, M. Nakajima, and T. Hamazaki (2009), Thermal and near infrared sensor for carbon observation Fourier-transform spectrometer on the Greenhouse Gases Observing Satellite for greenhouse gases monitoring, *Appl. Opt.*, *48*, 6716, doi:10.1364/AO.48.006716.

Lamouroux, J., H. Tran, A. L. Laraia, R. R. Gamache, L. S. Rothman, I. E. Gordon, and J. Hartmann (2010), Updated database plus software for line-mixing in CO_2 infrared spectra and their test using laboratory spectra in the 1.5-2.3 μm region, *J. Quant. Spectrosc. Radiat. Transfer*, *111*, 2321–2331, doi:10.1016/j.jqsrt.2010.03.006.

Meirink, J. F., H. J. Eskes, and A. P. H. Goede (2006), Sensitivity analysis of methane emissions derived from SCIAMACHY observations through inverse modelling, *Atmos. Chem. Phys.*, *6*, 1275–1292.

Messerschmidt, J., R. Macatangay, J. Notholt, C. Petri, T. Warneke, and C. Weinzierl (2010), Side by side measurements of CO_2 by ground-based Fourier transform spectrometry (FTS), *Tellus, Ser. B*, *62*, 749–758, doi:10.1111/j.1600-0889.2010.00491.x.

Morino, I., et al. (2011), Preliminary validation of column-averaged volume mixing ratios of carbon dioxide and methane retrieved from GOSAT short-wavelength infrared spectra, *Atmos. Meas. Tech.*, *4*, 1061–1076, doi:10.5194/amt-4-1061-2011.

Peters, W., et al. (2007), An atmospheric perspective on North American carbon dioxide exchange: CarbonTracker, *Proc. Natl. Acad. Sci. U. S. A.*, *104*, 18,925–18,930.

Reuter, M., et al. (2011), Retrieval of atmospheric CO_2 with enhanced accuracy and precision from SCIAMACHY: Validation with FTS measurements and comparison with model results, *J. Geophys. Res.*, *116*, D04301, doi:10.1029/2010JD015047.

Rothman, L. S., et al. (2009), The HITRAN 2008 molecular spectroscopic database, *J. Quant. Spectrosc. Radiat. Transfer*, *110*, 533–572, doi:10.1016/j.jqsrt.2009.02.013.

Tran, H., and J.-M. Hartmann (2008), An improved O_2A band absorption model and its consequences for retrievals of photon paths and surface pressures, *J. Geophys. Res.*, *113*, D18104, doi:10.1029/2008JD010011.

Wunch, D., et al. (2010), Calibration of the total carbon column observing network using aircraft profile data, *Atmos. Meas. Tech.*, *3*(5), 1351–1362, doi:10.5194/amt-3-1351-2010.

Wunch, D., G. C. Toon, J.-F. L. Blavier, R. Washenfelder, J. Notholt, B. J. Connor, D. W. T. Griffith, V. Sherlock, and P. O. W. Wennberg (2011), The total carbon column observing network, *Philos. Trans. R. Soc. A*, *369*, 2087–2112, doi:10.1098/rsta.2010.0240.

Yoshida, Y., Y. Ota, N. Eguchi, N. Kikuchi, K. Nobuta, H. Tran, I. Morino, and T. Yokota (2011), Retrieval algorithm for CO_2 and CH_4 column abundances from short-wavelength infrared spectral observations by the greenhouse gases observing satellite, *Atmos. Meas. Tech.*, *4*(4), 717–734, doi:10.5194/amt-4-717-2011.

I. Aben, A. Galli, S. Guerlet, O. Hasekamp, and D. Schepers, Netherlands Institute for Space Research, Utrecht, Netherlands.

A. Butz, Institute for Meteorology and Climate Research, Karlsruhe Institute of Technology, Campus Nord, H.-v.-Helmholtz-Platz 1, D-76344 Leopoldshafen, Germany. (andre.butz@kit.edu)

N. Deutscher, D. Griffith, and R. Macatangay, Center for Atmospheric Chemistry, University of Wollongong, Wollongong, NSW 2522, Australia.

C. Frankenberg and G. Toon, Jet Propulsion Laboratory, California Institute of Technology, M/S 183-601, 4800 Oak Grove Dr., Pasadena, CA 91109, USA.

J.-M. Hartmann and H. Tran, Laboratoire Interuniversitaire des Systèmes Atmosphériques, UMR 7583, CNRS, Université Paris Est Créteil, Université Paris Diderot Institut Pierre-Simon Laplace, F-94010 Créteil CEDEX, France.

G. Keppel-Aleks, P. Wennberg, and D. Wunch, Division of Engineering and Applied Science, California Institute of Technology, MC 150-21, Pasadena, CA 91125, USA.

A. Kuze, Satellite Applications and Promotion Center, Japan Aerospace Exploration Agency, 2-1-1 Sengen, Tsukuba, Ibaraki 305-8505, Japan.

J. Messerschmidt, J. Notholt, and T. Warneke, Institute of Environmental Physics, University of Bremen, Otto-Hahn-Allee 1, D-28359 Bremen, Germany.